AEGIS-K code for linear kinetic analysis of toroidally axisymmetric plasma stability

L.J. Zheng *, M.T. Kotschenreuther, J.W. Van Dam

Institute for Fusion Studies, University of Texas at Austin, Austin, TX 78712, United States

ABSTRACT

A linear kinetic stability code for tokamak plasmas: AEGIS-K (Adaptive EiGenfunction Independent Solutions-Kinetic), is described. The AEGIS-K code is based on the newly developed gyrokinetic theory [L.J. Zheng, M.T. Kotschenreuther, J.W. Van Dam, Phys. Plasmas 14 (2007) 072505]. The success in recovering the ideal magnetohydrodynamics (MHD) from this newly developed gyrokinetic theory in the proper limit leads the AEGIS-K code to be featured by being fully kinetic in essence but hybrid in appearance. The radial adaptive shooting scheme based on the method of the independent solution decomposition in the MHD AEGIS code [L.J. Zheng, M.T. Kotschenreuther, J. Comp. Phys. 211 (2006) 748] is extended to the kinetic calculation. A numerical method is developed to solve the gyrokinetic equation of lowest order for the response to the independent solutions of the electromagnetic perturbations, with the quasineutrality condition taken into account. A transform method is implemented to allow the pre-computed Z-function (i.e., the plasma dispersion function) to be used to reduce the integration dimension in the moment calculation and to assure the numerical accuracy in determining the wave–particle resonance effects. Periodic boundary condition along the whole banana orbit is introduced to treat the trapped particles, in contrast to the usual reflection symmetry conditions at the banana tips. Due to the adaptive feature, the AEGIS-K code is able to resolve the coupling between the kinetic resonances and the shear Alfvén continuum damping. Application of the AEGIS-K code to compute the resistive wall modes in ITER is discussed.

© 2010 Elsevier Inc. All rights reserved.

1. Introduction

The linear magnetohydrodynamic (MHD) stability codes, such as PEST, ERATO, GATO, DCON, AEGIS, MARG2D, MISHKA, etc. [1–9], have been proved to be important for tokamak physics studies. For magnetically confined plasmas, charged particles are sticked on the magnetic field lines to the leading order in the finite Larmor radius (FLR) expansion. This makes the brevity MHD model capture the dominant feature of the complicated many charged particle problem in the direction perpendicular to the magnetic field line. However, the particle movements in the direction parallel to the magnetic field line are not localized. Kinetic description is necessary in this direction. There is long history in studying the kinetic effects on the MHD modes. The recent discovery of the stabilization of resistive wall modes (RWMs) by the kinetic and shear Alfvén resonances has stimulated the global computational studies of resistive wall modes by taking into account the non-ideal MHD effects [10–14].

Due to the complexity of the global computation of the kinetic effects on MHD modes, several kinetic MHD codes based the perturbed numerical scheme have been developed, for example NOVA-K [15], the code combining MISHIKA and HAGIS

[9,16], and the code based on PEST [17]. The perturbed numerical scheme uses the ideal MHD eigen functions to evaluate the kinetic energy perturbatively and therefore cannot take into account the kinetic effects consistently. The effort to develop the non-perturbative code has been made in MARS-K code [18]. The current AEGIS-K (Adaptive EiGenfunction Independent Solutions-Kinetic) code is another effort in this direction with different underlying set of equations and new numerical scheme.

In the aspect of the underlying equations, we avoid the hybrid method used so far in this field, for example by MARS-K code [18]. In Ref. [19], we have successfully reformulated the gyrokinetic theory so that the MHD equations can be recovered in the proper limit. The current AEGIS-K code is based on this new gyrokinetic formalism. This makes our AEGIS-K code to be featured by being fully kinetic in essence but hybrid in appearance. For simplicity, in the current AEGIS-K effort we drop the FLR effects and concentrate to study all remaining kinetic effects: such as the kinetic resonance, trapped particle, and parallel electric field effects. Even in this lowest order description, our formalism is significantly different from the conventional gyrokinetic (in lowest order) or drift kinetic formalism. In the direction perpendicular to the magnetic field we found that the Pfirsch–Schlüter current effect has not been kept completely in the conventional gyrokinetic formalism. In the direction parallel to the magnetic field, we found that the coupling of the gyrophase-dependent part of the distribution function needs to be taken into account to derive the gyrokinetic equation of the lowest order (i.e., the drift kinetic equation). Only this coupling is taken into consideration properly, the structure of the MHD equation in the direction parallel to the magnetic field can be recovered in the proper fluid limit. In addition, we also include the parallel electric field effect by introducing the quasineutrality condition, which is another feature of AEGIS-K code.

In the aspect of the numerical scheme, we employ the radially adaptive shooting scheme by extending the MHD AEGIS numerical algorithm to the current kinetic one. The adaptive computation of MHD modes is vitally important to achieve the numerical accuracy. This is because the kinetic and shear Alfvén resonances can couple each other at the resonance magnetic surfaces. The importance of the adaptive scheme can be seen by inspecting the GATO grid density [5]. From GATO computation experience, the maximum number of the radial grid with the good numerical convergency (packed on the rational surfaces) is roughly 500 for up-down symmetric equilibrium. In the kinetic computation the eigen function is complex and therefore the matrix size is about four times larger. Furthermore, the MHD matrix is Hermitian, but the kinetic one not. All of these make the numerical convergency in the grid method a tough task for the kinetic computation . In the AEGIS formalism, however, the radial direction is based on the adaptive shooting of the independent solutions. Increasing the radial resolution does not increase the eigen matrix size. Our computation shows that the minimum radial resolution has to be over 600 grid points with packing at the resonance surfaces. This shows the advantage of the current adaptive numerical scheme. With such high radial resolution required, it would be hard for radially grid based kinetic codes, e.g., MARS-K code [18], to resolve kinetic and Alfvén resonances while ensuring the numerical convergence.

We also improve the numerical scheme in several other aspects. For example, a new transform technique is developed to solve the integro-differential gyrokinetic equations, that allows the pre-computed Z-function (i.e., the plasma dispersion function) [21] to be used to reduce the integration dimension in the kinetic moment calculation, and the periodic boundary conditions around the banana orbits are used to compute the trapped particle effects, etc.

The paper is arranged as follows: In Section 2 the equilibrium calculation is outlined. In Section 3 the eigen-value problem is formulated. In Section 4 the numerical results are given. In the last section the conclusions and discussion are presented.

2. Equilibrium

For simplicity we consider the axisymmetric systems and assume that the system is up-down symmetric. The equilibrium calculation is similar to that of the AEGIS code [7]. For toroidally symmetric configurations the magnetic filed $\vec{B}$ can be expressed as

$$\vec{B} = \chi' \mathbf{\nabla}\phi \times \mathbf{\nabla}\psi + g\mathbf{\nabla}\phi = \chi'(\mathbf{\nabla}\zeta \times \mathbf{\nabla}\psi + q\mathbf{\nabla}\psi \times \mathbf{\nabla}\theta),$$

where ϕ is the axisymmetric toroidal angle, θ and ζ are generalized poloidal and toroidal angles, respectively, ψ labels the magnetic surface, $\chi(\psi)$ denotes the poloidal magnetic flux, $g(\chi)$ is the poloidal current flux, q represents the safety factor, and prime denotes derivative with respect to ψ. Here and later on in this paper, the arrow is used to represent the vector in the configuration space. The poloidal flux χ is governed by the Grad–Shafranov equation, with the pressure profile $P(\chi)$ and poloidal current flux $g(\chi)$ specified. The Grad–Shafranov equation usually needs to be solved numerically by the equilibrium codes, for example TOQ (the MHD equilibrium code developed at General Atomics, San Diego, CA). The numerical equilibrium data, computed for example by TOQ, is the input to the AEGIS-K code. The data required by the AEGIS-K code are as follows: The profile functions including the poloidal magnetic flux $\chi(\psi)$, the pressure $P(\psi)$, and the poloidal current flux $g(\psi)$, and the flux coordinates: $X(\psi,\theta)$ and $Z(\psi,\theta)$ at grids, where X and Z are the Cartesian coordinates at $\phi = const$ plane. The AEGIS-K code performs re-griding both for radial coordinate and poloidal angle. The re-griding relies on the spline interpolations of the equilibrium data. As proposed in the PEST code [1] the coordinate splines are established on the generalized polar coordinate system. During the re-griding, choice is made available with respect to various coordinate systems, such as the PEST [1], Hamada [22], and the equal-arclength coordinate systems.

Here, we note that, since we have assumed that the equilibrium has perfect magnetic surfaces, the treatment of X-points has not been considered in our current version of AEGIS-K code. Nevertheless, AEGIS-K code can approach rather closely to the X-points by introducing more Fourier harmonics. Since AEGIS-K uses the radial independent solution method, its matrix

size is much smaller than that in the radial grid based codes. Therefore, AEGIS-K formalism allows considerably more poloidal Fourier harmonics to be added.

The Jacobian of the equilibrium coordinate system is defined as follows

$$J = \frac{1}{\mathbf{\nabla}\psi \times \mathbf{\nabla}\theta \cdot \mathbf{\nabla}\zeta}.$$

We also introduce the equilibrium matrices

$$
\begin{aligned}
G_{11} &= J(\mathbf{\nabla}\theta \times \mathbf{\nabla}\zeta) \cdot (\mathbf{\nabla}\theta \times \mathbf{\nabla}\zeta),\\
G_{22} &= J(\mathbf{\nabla}\zeta \times \mathbf{\nabla}\psi) \cdot (\mathbf{\nabla}\zeta \times \mathbf{\nabla}\psi),\\
G_{33} &= J(\mathbf{\nabla}\psi \times \mathbf{\nabla}\theta) \cdot (\mathbf{\nabla}\psi \times \mathbf{\nabla}\theta),\\
G_{12} &= J(\mathbf{\nabla}\theta \times \mathbf{\nabla}\zeta) \cdot (\mathbf{\nabla}\zeta \times \mathbf{\nabla}\psi),\\
G_{31} &= J(\mathbf{\nabla}\psi \times \mathbf{\nabla}\theta) \cdot (\mathbf{\nabla}\theta \times \mathbf{\nabla}\zeta),\\
G_{23} &= J(\mathbf{\nabla}\zeta \times \mathbf{\nabla}\psi) \cdot (\mathbf{\nabla}\psi \times \mathbf{\nabla}\theta).
\end{aligned}
$$

Beside these metric parameters the following decomposition of the curvature of the equilibrium magnetic field lines $\vec{\kappa}$ is also introduced:

$$\vec{\kappa} \times \vec{B} = K_s \vec{B} \times \vec{s} + K_\psi \mathbf{\nabla}\psi \times \vec{B}, \tag{1}$$

where $\vec{s} = \chi'(\mathbf{\nabla}\zeta - q\mathbf{\nabla}\theta)$.

3. Eigen-value problem

In this section the eigen-value problem is constructed. In difference from the ideal MHD case, the current kinetic problem is non-Hermitian. The whole system consist of the plasma, inter vacuum, resistive wall, and outer vacuum regions. For simplicity, it is assumed that the wall is thin. We denote respectively the interfaces between the plasma and the inner vacuum regions, the inner vacuum region and the wall, and the wall and the outer vacuum region as ψ_a, ψ_{b-}, and ψ_{b+}. We focus our attention on the plasma region, where the kinetic effects take place, while briefly outline the vacuum and wall description.

3.1. The matrix description of the plasma region

In this subsection we first give our basic set of equations and then describe the solution of the gyrokinetic equation and construction of the compressibility part of the pressure tensor. The set of the Euler–Lagrange equations for plasma region will be given at the end.

3.1.1. The basic set of equations for plasma region

We use our newly developed gyrokinetic formalism in Ref. [19] for constructing our basic set of equations. Having recovered the MHD from this formalism, we are able to study the MHD modes in a non-hybrid manner. We assume the mode frequency ω is larger than the ion diamagnetic drift frequency but smaller than the electron bounce frequency. The basic set of equations for AEGIS-K code is as follows: the perpendicular momentum equation

$$-\rho_m \hat{\omega}^2 \vec{\xi} = \delta\vec{J} \times \vec{B} + \vec{J} \times \delta\vec{B} - \mathbf{\nabla}\delta p_c - \mathbf{\nabla}_\perp \delta p_k, \tag{2}$$

the gyrophase-independent part of the gyrokinetic equation for ion species

$$\mathbf{v}_\parallel \cdot \mathbf{\nabla}\delta f - i\hat{\omega}\delta f = i\hat{\omega}\frac{m_\rho}{T_i}\mu B F_{g0}\mathbf{\nabla}_\perp \cdot \vec{\xi} + i\hat{\omega}\frac{m_\rho}{T_i}(\mu B - v_\parallel^2)F_{g0}\vec{\kappa} \cdot \vec{\xi} - i\hat{\omega}\frac{Ze_i}{T_i}F_{g0}\delta\varphi, \tag{3}$$

and the quasineutrality condition

$$\delta\varphi = -\frac{1}{1+Z\tau}\frac{T_e}{Ze_i}\frac{1}{n_0}\int d^3 v \delta f. \tag{4}$$

Here, $\vec{\xi}$ is the perpendicular field line displacement, $\delta p_c = -\vec{\xi} \cdot \mathbf{\nabla}P, \delta p_k = \int d^3 v(m_\rho \mu B)\delta f$, P represents the equilibrium pressure, ρ_m is the mass density, m_ρ denotes the mass, e_i is the ion charge, Z is the charge number, n_0 is the ion density, $\vec{B}$ denotes the equilibrium magnetic field, $\delta\vec{B} = \mathbf{\nabla} \times \vec{\xi} \times \vec{B}, \delta\vec{J} = \mathbf{\nabla} \times \delta\vec{B}$, v is the ion speed, $\mu = v_\perp^2/2B$ is the magnetic moment, T represents the temperature, $\tau = T_i/T_e$ with subscripts i and e represents respectively the ion and electron species. $\vec{\kappa}$ represents the field line curvature, $\delta\varphi$ specifies the parallel electric field effect, δf denotes the gyrophase averaged distribution function for ion species, F_{g0} is the Maxwellian distribution function, and the subscripts $\perp$ and $\parallel$ represent respectively the perpendicular and the parallel components to the equilibrium magnetic field line. Due to the assumption that the mode frequency is lower than the electron bounce frequency, we can assume that the electron response to be adiabatic. We denote the particle energy with E and the pitch angle with $\lambda = \mu/E$.

We assume rotation frequency Ω to be modestly low, i.e., much smaller than the parallel ion acoustic frequency but larger than the ion diamagnetic drift frequency. By assuming that the rotation frequency is larger than the ion diamagnetic drift frequency, we can avoid to treat the finite Larmor radius effects, especially the resonance effects with the ion precessional drift [17]. We consider only the case with rotation frequency smaller than the parallel ion acoustic frequency, since it is more interesting for ITER. Consequently, we can include the rotation effects simply by introducing the Doppler shift: i.e., by replacing the mode frequency ω (or growth rate γ) with $\hat{\omega} = i\hat{\gamma} \equiv \omega + n\Omega$ in Eqs. (2)–(4), where n is the toroidal mode number. The particle drift effects due to the centrifugal and Coriolis forces are negligible in this case.

Our representation of perturbed magnetic field $\delta\vec{B} = \mathbf{\nabla} \times \vec{\xi} \times \vec{B}$ is MHD-like. It holds only for plasmas without resistivity. In Ref. [19], we have proposed an alternative representation $\delta\vec{B} = g\mathbf{\nabla} \times \vec{\zeta} \times \nabla\phi$ that can avoid this limitation. However, in order to make apparent the eigen-function benchmark with existing ideal MHD codes, we have used MHD-like representation in our current work.

In our set of equations the wave-particle resonances, the shear Alfvén continuum damping, the trapped particle effect, and the parallel electric effects are all taken into account, while the FLR effects are dropped in our current effort. Even in this limit our starting equations are different from those of the conventional drift kinetic formalism. In the conventional derivation of the drift kinetic equation, the coupling between the gyrophase-averaged part and the gyrophase-dependent part of the gyrokinetic distribution function through the term $\dot{\alpha}_1 \partial\delta f/\partial\alpha$ has not been taken into account. Here, δf is the distribution function and α is the gyrophase, with the subscript "1" denoting the first-order and the dot representing the time derivative along the unperturbed particle orbit. Actually, only if this coupling is taken into account, the parallel MHD equation of motion can be retrieved in the proper limit. This coupling can be, alternatively, taken into account by including α_1 into the generalized gyrophase definition.

We have not considered the precessional drift resonance either, since we note that considering the resonance alone is insufficient for ordering consistency. Since $\langle\omega_d\rangle/\omega_{*i} \sim a/R$, inclusion of the $\langle\omega_d\rangle$ effect also needs to take into account the ω_{*i} effect (i.e., $k_\perp^2 \rho_i^2$ effects) for consistency. Here, $\langle\omega_d\rangle$ is the processional drift frequency, ω_{*i} is the ion diamagnetic drift frequency, $k_\perp$ represents the perpendicular wave number, and ρ_i is the ion gyro radius. Due to this complexity, we postpone this part of the work to the future studies.

Here, let us also outline the decompositions for the perturbations. The magnetic field line displacement is decomposed as follows [6]

$$\vec{\xi} \times \vec{B} = \xi_s \mathbf{\nabla}\psi + \xi_\psi \chi'(\mathbf{\nabla}\zeta - q\mathbf{\nabla}\theta). \tag{5}$$

Since we deal with the linear problem, the Fourier transform method can be used to decompose the perturbed quantities in the poloidal and toroidal directions, for example

$$\xi \exp\{-in\zeta\} = \sum_{m=-\infty}^{\infty} \xi_m \frac{1}{\sqrt{2\pi}} \exp\{i(m\theta - n\zeta)\}, \tag{6}$$

with

$$\xi_m = \int_{-\pi}^{\pi} d\theta\,\xi \frac{1}{\sqrt{2\pi}} \exp\{-im\theta\}.$$

With the toroidal symmetry assumed, only a single toroidal Fourier component needs to be considered. As usual, the equilibrium quantities can be decomposed as the matrices in the poloidal Fourier space, for example

$$\mathcal{J}_{mm'} = \frac{1}{2\pi} \int_{-\pi}^{\pi} d\theta J(\theta) e^{i(m-m')\theta}.$$

In the poloidal Fourier decomposition, the Fourier components are cut off both from the lower and upper sides respectively by m_{min} and m_{max}. Therefore, the total Fourier component under consideration is $M = m_{max} - m_{min} + 1$. We use the bold face (or alternatively $[[\cdots]]$) to represent the vector (e.g., $\boldsymbol{\xi}$) and the calligraphic capital letters (or alternatively $\langle\cdots\rangle$) to represent the corresponding equilibrium matrices (e.g., $\mathcal{J}$ for J) in the poloidal Fourier space.

3.1.2. Solution of the gyrokinetic equation

In this sub-subsection we describe the solution of the gyrokinetic equation. Using the decompositions in Eqs. (1) and (5), the gyrokinetic equation in Eq. (3) is reduced to

$$\sigma_\parallel \sqrt{2}\sqrt{E}\sqrt{1-\lambda B} \frac{\chi'}{\mathcal{J}B} \frac{\partial}{\partial\theta}\delta f - in\sigma_\parallel \sqrt{2}q\sqrt{E}\sqrt{1-\lambda B} \frac{\chi'}{\mathcal{J}B}\delta f - i(\omega + n\Omega)\delta f$$
$$= i(\omega + n\Omega)\left\{\frac{m_\rho E}{T_i}F_{g0}(R_s\xi_s + R_1\xi'_\psi + R_0\xi_\psi) + \frac{Z\tau}{1+Z\tau}F_{g0}R_\varphi\delta\varphi\right\}, \tag{7}$$

where $R_s = iR_s^e + R_s^o, R_0 = -iR_0^o + R_0^e$, and

$$R_s^e = \frac{\chi'}{\mathcal{J}B^2}[n(G_{22} + qG_{23}) + (G_{23} + qG_{33})m]\lambda B,$$

$$R_s^o = K_s(\lambda B - 2),$$

$$R_1 = \frac{\chi'^2}{\mathcal{J}B^2}[(G_{22} + qG_{23}) + q(G_{23} + qG_{33})]\lambda B,$$

$$R_0^e = \left\{\frac{\chi'}{\mathcal{J}B^2}[\chi''(G_{22} + qG_{23}) + (q\chi')'(G_{23} + qG_{33})] + \frac{\mu_0 P'}{B^2}\right\}\lambda B + K_\psi(\lambda B - 2),$$

$$R_0^o = \frac{\chi'^2}{\mathcal{J}B^2}(G_{12} + qG_{31})(m - nq).$$

Here, $\sigma_\parallel$ represents the sign of the parallel velocity. Note that the electric potential $\delta\varphi$ depends on the distribution function δf. Eq. (7) is actually an integro-differential equation.

To solve the gyrokinetic Eq. (7), one needs to specify the boundary condition for trapped particles. The conventional condition for trapped particles is that $f(\sigma_\parallel > 0) = f(\sigma_\parallel < 0)$ at the turning points, i.e., the reflection symmetry: the trapped particles approaching to the turning points equal to those leaving from the points. To establish an unified treatment for circulating and trapped particles, we consider the period boundary condition for a trapped particle along its complete banana orbit, which can be proved to be equivalent to the conventional boundary condition.

We introduce the following coordinate transform both for circulating and trapped particles:

$$\hat{\theta}(\lambda, \theta) = \frac{2\pi}{\tau_c \chi'}\int_0^\theta \frac{\mathcal{J}Bd\theta}{\sqrt{1 - \lambda B}},$$

where the range of $\hat{\theta}$ is from 0 to 2π. The bounce time τ_c is defined differently for circulating particles

$$\tau_c(\lambda) = 2\frac{1}{\chi'}\int_0^\pi \frac{\mathcal{J}Bd\theta}{\sqrt{1 - \lambda B}};$$

and for trapped particles

$$\tau_c(\lambda) = 4\frac{1}{\chi'}\int_0^{\theta_t} \frac{\mathcal{J}Bd\theta}{\sqrt{1 - \lambda B}}.$$

In order to use directly the plasma dispersion function (Z-function) for energy integration in the moment calculations, we introduce the transform

$$\delta f = \delta\hat{f}e^{inq(\theta - \hat{\theta})}.$$

Therefore, the gyrokinetic equation Eq. (7) becomes

$$\sigma_\parallel 2\sqrt{2}\pi\frac{1}{\tau_c}\sqrt{E}\frac{\partial\delta\hat{f}}{\partial\hat{\theta}} - i\sigma_\parallel 2\sqrt{2}\pi nq\frac{1}{\tau_c}\sqrt{E}\delta\hat{f} - i(\omega + n\Omega)\delta\hat{f}$$
$$= i(\omega + n\Omega)e^{-inq(\theta - \hat{\theta})}\left[\frac{m_\rho E}{T_i}F_{g0}(R_s\xi_s + R_1\xi'_\psi + R_0\xi_\psi) + \frac{Z\tau}{1 + Z\tau}F_{g0}R_\varphi\delta\varphi\right]. \tag{8}$$

To solve the gyrokinetic Eq. (8), we decompose the distribution function into the $\hat{\theta}$ space Fourier series:

$$\delta\hat{f} = \frac{1}{\sqrt{2\pi}}\sum_{-\infty}^{+\infty}\delta\hat{f}_{\hat{m}}\exp\{i\hat{m}\hat{\theta}\}. \tag{9}$$

Using transforms for $\delta\hat{f}$ in Eq. (9) and for $\vec{\xi}$ in Eq. (6), the gyrokinetic equation in (8) can be formally solved

$$\delta\hat{f}_{\hat{m}} = (\omega + n\Omega)\sum_m \left\{\frac{m_\rho}{T_i}(R_{s,\hat{m}m}\xi_{s,m} + R_{1,\hat{m}m}\xi'_{\psi,m} + R_{0,\hat{m}m}\xi_{\psi,m}) \times \frac{EF_{g0}}{\sigma_\parallel 2\sqrt{2}\pi\frac{1}{\tau_c}\sqrt{E}(\hat{m} - nq) - (\omega + n\Omega)} \right.$$
$$\left. + \frac{Z\tau}{1 + Z\tau}R_{\varphi,\hat{m}m}\delta\varphi_m\frac{F_{g0}}{\sigma_\parallel 2\sqrt{2}\pi\frac{1}{\tau_c}\sqrt{E}(\hat{m} - nq) - (\omega + n\Omega)}\right\}, \tag{10}$$

where for circulating particles

$$R_{s,\hat{m}m}(\lambda) = i\frac{1}{\pi}\int_0^\pi d\hat{\theta}\{R_s^e\cos[(m-nq)\theta - (\hat{m}-nq)\hat{\theta}] + R_s^o\sin[(m-nq)\theta - (\hat{m}-nq)\hat{\theta}]\},$$

$$R_{1,\hat{m}m}(\lambda) = \frac{1}{\pi}\int_0^\pi d\hat{\theta}R_1\cos[(m-nq)\theta - (\hat{m}-nq)\hat{\theta}],$$

$$R_{0,\hat{m}m}(\lambda) = \frac{1}{\pi}\int_0^\pi d\hat{\theta}\{R_0^e\cos[(m-nq)\theta - (\hat{m}-nq)\hat{\theta}] + R_0^o\sin[(m-nq)\theta - (\hat{m}-nq)\hat{\theta}]\},$$

$$R_{\varphi,\hat{m}m}(\lambda) = \frac{1}{\pi}\int_0^\pi d\hat{\theta}\cos[(m-nq)\theta - (\hat{m}-nq)\hat{\theta}],$$

and for trapped particles

$$R_{s,\hat{m}m}(\lambda) = i\frac{2}{\pi}\int_0^{\pi/2} d\hat{\theta}\{R_s^e\cos[(m-nq)\theta - (\hat{m}-nq)\hat{\theta}] + R_s^o\sin[(m-nq)\theta - (\hat{m}-nq)\hat{\theta}]\},$$

$$R_{1,\hat{m}m}(\lambda) = \frac{2}{\pi}\int_0^{\pi/2} d\hat{\theta}R_1\cos[(m-nq)\theta - (\hat{m}-nq)\hat{\theta}],$$

$$R_{0,\hat{m}m}(\lambda) = \frac{2}{\pi}\int_0^{\pi/2} d\hat{\theta}\{R_0^e\cos[(m-nq)\theta - (\hat{m}-nq)\hat{\theta}] + R_0^o\sin[(m-nq)\theta - (\hat{m}-nq)\hat{\theta}]\},$$

$$R_{\varphi,\hat{m}m}(\lambda) = \frac{2}{\pi}\int_0^{\pi/2} d\hat{\theta}\cos[(m-nq)\theta - (\hat{m}-nq)\hat{\theta}].$$

3.1.3. Pressure moment and quasineutrality condition

In this sub-subsection, we construct pressure and density moments using the solution of the gyrokinetic equation obtained in the last sub-subsection. Using the energy and pitch angle as variables, the perturbed kinetic pressure can be expressed as

$$\delta p_k = 2\sqrt{2}\pi m_\rho B^2 \int \frac{d\lambda dE}{\sqrt{1-\lambda B}} E^{3/2}\lambda \frac{\delta f_+ + \delta f_-}{2}.$$

Here, the subscript + and − represent the sign of the parallel velocity for circulating particles. For trapped particles, however, + represents the counter-clockwise orbits, while – clockwise ones. Introducing Fourier decomposition in Eq. (6), we obtain the vector equation in the Fourier space for kinetic pressure:

$$\{\delta p_k\}_{m'} = n_0 T_i \frac{1}{\sqrt{2\pi}}\int_0^{2\pi} d\theta B^2 e^{-im'\theta}\int_0^{1/B} d\lambda \frac{\lambda}{\sqrt{1-\lambda B}}\frac{2\sqrt{2}\pi}{n_0}\frac{m_\rho}{T_i}\int_0^\infty dE E^{3/2}\frac{\delta f_+ + \delta f_-}{2}.$$

Inserting the solution of the gyrokinetic equation Eq. (10), one obtains

$$\boldsymbol{\delta p_k} = n_0 T_i(\mathcal{P}_s\boldsymbol{\xi}_s + \mathcal{P}_1\boldsymbol{\xi}_\psi' + \mathcal{P}_0\boldsymbol{\xi}_\psi + \mathcal{P}_\varphi\boldsymbol{\delta\varphi}), \tag{11}$$

where the elements of pressure response matrices are given as follows

$$\mathcal{P}_{(s,1,0),m'm} = \sqrt{\frac{2}{\pi}}\int_0^\pi d\theta B^2 \int_0^{1/B} d\lambda \frac{\lambda}{\sqrt{1-\lambda B}}\sum_{\hat{m}} R_{(s,1,0),\hat{m},m}(\lambda)\cos[(\hat{m}-nq)\hat{\theta} - (m'-nq)\theta]g_3(\zeta(\tau_c(\lambda),\hat{m})),$$

$$\mathcal{P}_{\varphi,m'm} = \frac{Z\tau}{1+Z\tau}\sqrt{\frac{2}{\pi}}\int_0^\pi d\theta B^2 \int_0^{1/B} d\lambda \frac{\lambda}{\sqrt{1-\lambda B}}\sum_{\hat{m}} R_{\varphi,\hat{m},m}(\lambda)\cos[(\hat{m}-nq)\hat{\theta} - (m'-nq)\theta]g_2(\zeta(\tau_c(\lambda),\hat{m})),$$

with

$$g_k = \zeta Z_k(\zeta),$$
$$Z_k(\zeta) = \frac{\zeta}{\sqrt{\pi}}\int_0^\infty dE\frac{E^{k-1/2}}{E-\zeta^2}e^{-E}, \tag{12}$$
$$\zeta = \frac{1}{\sqrt{\beta_0}R_0 q_0}\frac{\hat{\omega}_N}{2\pi(\hat{m}-nq)\sqrt{T_i/T_{i0}}/\tau_c}.$$

Here, k is integer, β represents the ratio of plasma to magnetic energies, R is the major radius, the subscript 0 denotes being at the magnetic axis, and the subscript N for frequency or growth rate denotes the normalization by the Alfvén frequency at the magnetic axis $1/\tau_A$. Note that with Z_0 is just the usual plasma Z-function [21].

Similarly, we can express the Fourier component of the perturbed electrostatic potential in the quasineutrality condition Eq. (4) as follows

$$\delta\varphi_m = \frac{1}{\sqrt{2\pi}}\int_{-\pi}^\pi d\theta B e^{-im'\theta}\int_0^{1/B} d\lambda \frac{1}{\sqrt{1-\lambda B}}\frac{2\sqrt{2}\pi}{n_0}\int_0^\infty dE E^{1/2}\frac{\delta f_+ + \delta f_-}{2}.$$

Inserting the solution of the gyrokinetic equation Eq. (10), one obtains

$$\delta\boldsymbol{\varphi} = \mathcal{E}_s\boldsymbol{\xi}_s + \mathcal{E}_1\boldsymbol{\xi}'_\psi + \mathcal{E}_0\boldsymbol{\xi}_\psi + \overline{\mathcal{E}}_\varphi\delta\boldsymbol{\varphi}, \tag{13}$$

where the matrix elements are given as follows

$$\mathcal{E}_{(s,1,0),m'm} = \sqrt{\frac{2}{\pi}}\int_0^\pi d\theta B \int_0^{1/B} d\lambda \frac{1}{\sqrt{1-\lambda B}}\sum_{\hat{m}} R_{(s,1,0),\hat{m},m}(\lambda)\cos[(\hat{m}-nq)\hat{\theta} - (m'-nq)\theta]f_2(\zeta(\tau_c(\lambda),\hat{m})),$$

$$\overline{\mathcal{E}}_{\varphi,m'm} = \frac{Z\tau}{1+Z\tau}\sqrt{\frac{2}{\pi}}\int_0^\pi d\theta B \int_0^{1/B} d\lambda \frac{1}{\sqrt{1-\lambda B}}\sum_{\hat{m}} R_{\varphi,\hat{m},m}(\lambda)\cos[(\hat{m}-nq)\hat{\theta} - (m'-nq)\theta]f_1(\zeta(\tau_c(\lambda),\hat{m})),$$

We can solve $\delta\boldsymbol{\varphi}$ in Eq. (13), yielding

$$\delta\boldsymbol{\varphi} = \mathcal{E}_\varphi^{-1}\mathcal{E}_s\boldsymbol{\xi}_s + \mathcal{E}_\varphi^{-1}\mathcal{E}_1\boldsymbol{\xi}'_\psi + \mathcal{E}_\varphi^{-1}\mathcal{E}_0\boldsymbol{\xi}_\psi,$$

where $\mathcal{E} = \mathcal{I} - \overline{\mathcal{E}}$ and $\mathcal{I}$ is the unitary matrix. Inserting this solution into Eq. (11), we finally get the kinetic-effect-induced pressure moment:

$$\delta\boldsymbol{p}_k = n_0T_i[(\mathcal{P}_s + \mathcal{P}_\varphi\mathcal{E}_\varphi^{-1}\mathcal{E}_s)\boldsymbol{\xi}_s + (\mathcal{P}_1 + \mathcal{P}_\varphi\mathcal{E}_\varphi^{-1}\mathcal{E}_1)\boldsymbol{\xi}'_\psi + (\mathcal{P}_0 + \mathcal{P}_\varphi\mathcal{E}_\varphi^{-1}\mathcal{E}_0)\boldsymbol{\xi}_\psi]. \tag{14}$$

3.1.4. Euler–Lagrange equations for plasma region

The pressure moment constructed in the last sub-subsection can be used to derive the Euler–Lagrange equations in the plasma region by reducing the perpendicular momentum Eq. (2). We first insert the kinetic-effect-induced pressure moment in Eq. (14) into Eq. (2), project the resulting equation respectively onto two directions $J^2\nabla\theta \times \nabla\zeta \cdot \vec{B}\times[\cdots\times\vec{B}]/B^2$ and $(1/q\chi')J^2\nabla\zeta \times \nabla\psi \cdot \vec{B}\times[\cdots\times\vec{B}]/B^2$, and then introduce the Fourier transformation in Eq. (6) to the two projected equations. These procedures lead to the following two sets of differential equations in matrices

$$(\mathcal{B}^L\boldsymbol{\xi}_s + \mathcal{D}\boldsymbol{\xi}'_\psi + \mathcal{E}\boldsymbol{\xi}_\psi)' - (\mathcal{C}^L\boldsymbol{\xi}_s + \mathcal{E}^L\boldsymbol{\xi}'_\psi + \mathcal{H}\boldsymbol{\xi}_\psi) = 0, \tag{15}$$

$$\mathcal{A}\boldsymbol{\xi}_s + \mathcal{B}\boldsymbol{\xi}'_\psi + \mathcal{C}\boldsymbol{\xi}_\psi = 0, \tag{16}$$

where the equilibrium matrices $(\mathcal{A}, \mathcal{B}, \text{etc.})$ are given in Appendix A.

The structure of the set of differential Eqs. (15) and (16) is same as the ideal MHD one, except the matrices becomes complex and non-conjugate. The procedure in MHD AEGIS code can be extended to solve this set of equations. We can reduce this set of equations into the set of the first-order differential equations as in the DCON formalism [6]. By solving Eq. (16), we obtain

$$\boldsymbol{\xi}_s = -\mathcal{A}^{-1}\mathcal{B}\boldsymbol{\xi}'_\psi - \mathcal{A}^{-1}\mathcal{C}\boldsymbol{\xi}_\psi.$$

Inserting this solution into Eq. (15), we get

$$\frac{d}{d\psi}(\mathcal{F}\boldsymbol{\xi}' + \mathcal{K}\boldsymbol{\xi}) - (\mathcal{K}^L\boldsymbol{\xi}' + \mathcal{G}\boldsymbol{\xi}) = 0, \tag{17}$$

where

$$\mathcal{F} = \mathcal{D} - \mathcal{B}^\dagger\mathcal{A}^{-1}\mathcal{B},$$
$$\mathcal{K} = \mathcal{E} - \mathcal{B}^L\mathcal{A}^{-1}\mathcal{C},$$
$$\mathcal{K}^L = \mathcal{E}^L - \mathcal{C}^L\mathcal{A}^{-1}\mathcal{B},$$
$$\mathcal{G} = \mathcal{H} - \mathcal{C}^L\mathcal{A}^{-1}\mathcal{C}.$$

These matrices can be further simplified, as detailed in Appendix B.

Introducing the expanded 2M unknowns $\mathbf{u} = \begin{pmatrix} \boldsymbol{\xi} \\ \mathbf{u}_2 \end{pmatrix}$, where $\mathbf{u}_2 = \mathcal{F}\boldsymbol{\xi}' + \mathcal{K}\boldsymbol{\xi}$, Eq. (17) is reduced to the set of 2M first-order equations

$$\mathbf{u}' = \mathcal{L}\mathbf{u}, \tag{18}$$

where $2M \times 2M$ matrix

$$\mathcal{L} = \begin{pmatrix} -\mathcal{F}^{-1}\mathcal{K} & \mathcal{F}^{-1} \\ \mathcal{G} - \mathcal{K}^L\mathcal{F}^{-1}\mathcal{K} & \mathcal{K}^L\mathcal{F}^{-1} \end{pmatrix}.$$

We note that $\boldsymbol{\xi}$ and $\mathbf{u}_2$ in the plasma region are related to the magnetic field and pressure as follows

$$[[\mathcal{J}\mathbf{\nabla}\psi \cdot \delta\vec{B}]] = i\mathcal{Q}\xi,$$

$$-[[\mathcal{J}(\vec{B}\cdot\delta\vec{B} - \vec{\xi}\cdot\mathbf{\nabla}P)]] = \mathbf{u}_2.$$

The set of the eigen mode equations in Eq. (18) can be solved by means of the independent solution method as described in Ref. [7]. With M boundary conditions imposed at the magnetic axis, there remain only M independent solutions:

$$\begin{pmatrix}\Xi_p \\ \mathcal{W}_2\end{pmatrix} \equiv \begin{pmatrix}\xi^1, & \cdots, & \xi^M \\ \mathbf{u}_2^1, & \cdots, & \mathbf{u}_2^M\end{pmatrix},$$

where the superscripts are used to label the independent solutions. As the ideal MHD case [7], we use the cylinder limit to describe the boundary condition at the magnetic axis, i.e., $\xi_{\psi,m} \propto r^m$. The general solution can be then obtained as a combination of the M independent solutions,

$$\begin{pmatrix}\xi \\ \mathbf{u}_2\end{pmatrix} = i\begin{pmatrix}\Xi_p \\ \mathcal{W}_p\end{pmatrix}\mathbf{c}_p,\tag{19}$$

where $\mathbf{c}_p$ is a constant vector with M elements. Without loss of generality (by defining $\mathbf{c}_p = \Xi_p^{-1}\mathbf{c}_p^{new}$ and $\mathcal{W}_p^{new} = \mathcal{W}_p\Xi_p^{-1}$), we can set Ξ_p to be unity $\mathcal{I}$. Therefore, we have

$$[[\mathcal{J}\mathbf{\nabla}\psi \cdot \delta\vec{B}]] = -\mathcal{Q}\mathbf{c}_p,\tag{20}$$

$$-[[\mathcal{J}(\vec{B}\cdot\delta\vec{B} - \vec{\xi}\cdot\mathbf{\nabla}P)]] = i\mathcal{W}_p\mathbf{c}_p.\tag{21}$$

3.2. The solution of the vacuum region

For completeness, in this subsection we briefly review the vacuum solutions in Ref. [7]. The vacuum regions are described by the Laplace equation

$$\mathbf{\nabla}^2 u = 0,\tag{22}$$

where u is the magnetic scalar potential and is related to the perturbed magnetic field by $\delta\vec{B} = -\mathbf{\nabla}u$. Here, we note that this representation of vacuum magnetic field, although being simple, excludes the consideration of $n = 0$ modes. To study $n = 0$ modes, one more scalar is needed to represent the vacuum magnetic field [20]. For the sake of conciseness, we outline the general solutions for the inner and outer vacuum regions simultaneously.

As in the plasma region, Fourier decompositions are introduced for both poloidal and toroidal directions to solve Eq. (22). Then Eq. (22) becomes a set of second-order differential equations of number M for $\mathbf{u}$. This set of second-order differential equations can be transformed into a set of first-order differential equations of number $2M$, by introducing a new field $\mathbf{v} = -[[\mathcal{J}\mathbf{\nabla}\psi \cdot \delta\vec{B}]]$, which is related to the magnetic scalar potential in Fourier space as follows:

$$\mathbf{v} = \langle\mathcal{J}|\mathbf{\nabla}\psi|^2\rangle\frac{\partial\mathbf{u}}{\partial\psi} + \langle i\mathcal{J}\mathbf{\nabla}\psi \cdot \mathbf{\nabla}\theta\rangle\mathcal{M}\mathbf{u}.$$

There are $2M$ independent solutions for Eq. (22), which can be used to construct the following independent solution matrices:

$$\begin{pmatrix}\mathcal{U}_1 \\ \mathcal{V}_1\end{pmatrix} \equiv \begin{pmatrix}\mathbf{u}^1,\ldots,\mathbf{u}^M \\ \mathbf{v}^1,\ldots,\mathbf{v}^M\end{pmatrix},$$

$$\begin{pmatrix}\mathcal{U}_2 \\ \mathcal{V}_2\end{pmatrix} \equiv \begin{pmatrix}\mathbf{u}^{M+1},\ldots,\mathbf{u}^{2M} \\ \mathbf{v}^{M+1},\ldots,\mathbf{v}^{2M}\end{pmatrix}.$$

The general solutions in the vacuum regions can be expressed as a linear combination of the independent solutions:

$$\begin{pmatrix}\mathbf{u} \\ \mathbf{v}\end{pmatrix} = \begin{pmatrix}\mathcal{U}_1 \\ \mathcal{V}_1\end{pmatrix}\mathbf{c}_v + \begin{pmatrix}\mathcal{U}_2 \\ \mathcal{V}_2\end{pmatrix}\mathbf{d}_v,\tag{23}$$

where $\mathbf{c}_v$ and $\mathbf{d}_v$ are constant vectors in the independent solution space. To distinguish the inner and outer vacuum solutions, we let $\mathbf{c}_{v1}$ and $\mathbf{d}_{v1}$ denote the constants for the inner vacuum region and $\mathbf{c}_{v2}$ and $\mathbf{d}_{v2}$ for the outer vacuum region.

In the outer vacuum region, the scalar potential $\mathbf{u}$ is subjected to M boundary conditions at infinite ψ. With these M boundary conditions imposed, there are only M independent solutions left. Without loss of generality, we can set $\mathbf{c}_{v2}$ to be zero in this case. Consequently, eliminating $\mathbf{d}_{v2}$ in Eq. (23), we obtain

$$\mathbf{u}|_{\psi_{b+}} = \mathcal{T}\mathbf{v}|_{\psi_{b+}},$$

where the $M \times M$ matrix $\mathcal{T}$ is given by $\mathcal{T} = \mathcal{U}_2\mathcal{V}_2^{-1}|_{\psi_{b+}}$. The matrix $\mathcal{T}$ can be computed by means of the Green function method [23].

In the inner vacuum region, the independent solutions can be constructed, for example, with the use of an inward numerical shooting [7], with the following boundary conditions imposed at ψ_{b-}:

$$\begin{pmatrix} \mathcal{U}_1 \\ \mathcal{V}_1 \end{pmatrix}_{\psi_{b-}} = \begin{pmatrix} \mathcal{I} \\ \mathcal{O} \end{pmatrix}, \tag{24}$$

$$\begin{pmatrix} \mathcal{U}_2 \\ \mathcal{V}_2 \end{pmatrix}_{\psi_{b-}} = \begin{pmatrix} \mathcal{T} \\ \mathcal{I} \end{pmatrix}, \tag{25}$$

where $\mathcal{O}$ is the $M \times M$ zero matrix. Since the boundary conditions in Eq. (24) give $\delta \vec{B} \cdot \nabla \psi = 0$ at the wall, these conditions correspond to a set of solutions that corresponds to the perfectly conducting wall type. On the other hand, since the boundary conditions in Eq. (25) guarantee that the independent solutions to be continuous with the outer vacuum solutions, these conditions correspond to a set of solutions that corresponds to the no-wall type. Using the general expression for the solutions in Eq. (23), we can express the normal and parallel magnetic fields at the plasma-vacuum interface as follows:

$$[[\mathcal{J} \nabla \psi \cdot \delta \vec{B}]] = -\mathcal{V}_1 \mathbf{c}_{\nu 1} - \mathcal{V}_2 \mathbf{d}_{\nu 1}, \tag{26}$$

$$- [[\mathcal{J} \vec{B} \cdot \delta \vec{B}]] = i\mathcal{Q}(\mathcal{U}_1 \mathbf{c}_{\nu 1} + \mathcal{U}_2 \mathbf{d}_{\nu 1}). \tag{27}$$

3.3. Eigen-value problem

The solutions in the plasma and vacuum regions described in the last two subsections can be used to construct the eigenvalue problem as in the ideal MHD case in Ref. [7]. The normal magnetic field component and the combined magnetic and thermal pressures are required to be continuous at the plasma-vacuum interface. Matching the plasma [Eqs. (20) and (21)] and the vacuum [Eqs. (26) and (27)] solutions at the interface ψ_a gives

$$\mathbf{d}_{\nu 1} = \mathcal{F}_1^{-1} \delta \mathcal{W}_b \delta \mathcal{W}_\infty^{-1} \mathcal{F}_2 \mathbf{c}_{\nu 1}, \tag{28}$$

where $\delta \mathcal{W}_\infty = \mathcal{W}_p - \mathcal{Q}[\mathcal{U}_2 \mathcal{V}_2^{-1}]_{\psi_a} \mathcal{Q}, \delta \mathcal{W}_b = \mathcal{W}_p - \mathcal{Q}[\mathcal{U}_1 \mathcal{V}_1^{-1}]_{\psi_a} \mathcal{Q}, \mathcal{F}_1 = \mathcal{Q}[\mathcal{U}_2 - \mathcal{U}_1 \mathcal{V}_1^{-1} \mathcal{V}_2]_{\psi_a}$, and $\mathcal{F}_2 = \mathcal{Q}[\mathcal{U}_1 - \mathcal{U}_2 \mathcal{V}_2^{-1} \mathcal{V}_1]_{\psi_a}$. Note that $\delta \mathcal{W}_\infty$ and $\delta \mathcal{W}_b$ correspond to the energy matrices without a wall and with a perfectly conducting wall at ψ_b, respectively, as can be seen from the boundary conditions in Eqs. (24) and (25).

We now consider the matching across the thin resistive wall. For the radial magnetic field, the Maxwell equation $\nabla \cdot \delta \vec{B} = 0$ and the thin wall assumption lead to

$$\mathbf{v}|_{\psi_{b-}} = \mathbf{v}|_{\psi_{b+}} = \mathbf{d}_{\nu 1}. \tag{29}$$

The current in the resistive wall causes a jump in the scalar magnetic potential. This can be obtained from the Ampére law

$$\nabla \times \nabla \times \delta \vec{B} = -\gamma \mu_0 \sigma \delta \vec{B}, \tag{30}$$

where σ is the wall conductivity. Eq. (30) can be reduced to

$$\mathcal{V}(\mathbf{u}|_{\psi_{b+}} - \mathbf{u}|_{\psi_{b-}}) = \tau_w \gamma_N \mathbf{d}_{\nu 1}, \tag{31}$$

where $\tau_w = \mu_0 \sigma db/\tau_A$, d is the wall thickness, b is the average wall minor radius, and

$$\mathcal{V} = \mathcal{M}\langle \mathcal{J}|\nabla \psi||\nabla \theta| - \mathcal{J}|\nabla \psi \cdot \nabla \theta|^2/(|\nabla \psi||\nabla \theta|)\rangle \mathcal{M} + n^2 \langle \mathcal{J}|\nabla \phi|^2 |\nabla \psi|/|\nabla \theta|\rangle.$$

Since $\mathbf{c}_{\nu 2} = 0$, we find that Eqs. (23)–(25) yield

$$\mathbf{u}|_{\psi_{b+}} - \mathbf{u}|_{\psi_{b-}} = -\mathbf{c}_{\nu 1}. \tag{32}$$

From Eqs. (28), (31), and (32) we find the eigen mode equations

$$\mathcal{D}_0(\gamma_N)\mathbf{d}_{\nu 1} \equiv \tau_w \gamma_N \mathbf{d}_{\nu 1} + \mathcal{V}\mathcal{F}_2^{-1}\delta \mathcal{W}_\infty \delta \mathcal{W}_b^{-1} \mathcal{F}_1 \mathbf{d}_{\nu 1} = \mathcal{O}.$$

The dispersion relation for this eigen-value problem is given by the determinant equation $\det |\mathcal{D}_0(\gamma_N)| = 0$. In general the Nyquist diagram can be used to determine the roots of this dispersion relation. For RWMs, however, the growth rate is much smaller than the Alfvén frequency. Therefore, the growth rate dependence of $\delta \mathcal{W}_\infty \delta \mathcal{W}_b^{-1}$ can be neglected for determining the stability condition. Consequently, one can use the reduced eigen-value problem

$$-\mathcal{V}\mathcal{F}_2^{-1}\delta \mathcal{W}_\infty \delta \mathcal{W}_b^{-1} \mathcal{F}_1 \mathbf{d}_{\nu 1} = \tau_w \gamma_N \mathbf{d}_{\nu 1}, \tag{33}$$

with the RWM mode growth rate γ_N on the right hand side of this equation used as the eigen-value to determine the stability.

4. Numerical results

In this section we will describe the numerical work to implement the theoretical formalism described in the previous section. Note that the vacuum and wall parts are basically the same as the ideal MHD case as described in Ref. [7], except the complex nature in the kinetic description. We therefore focus ourselves on describing the plasma region. We have used the NAG mathematics library to build our code.
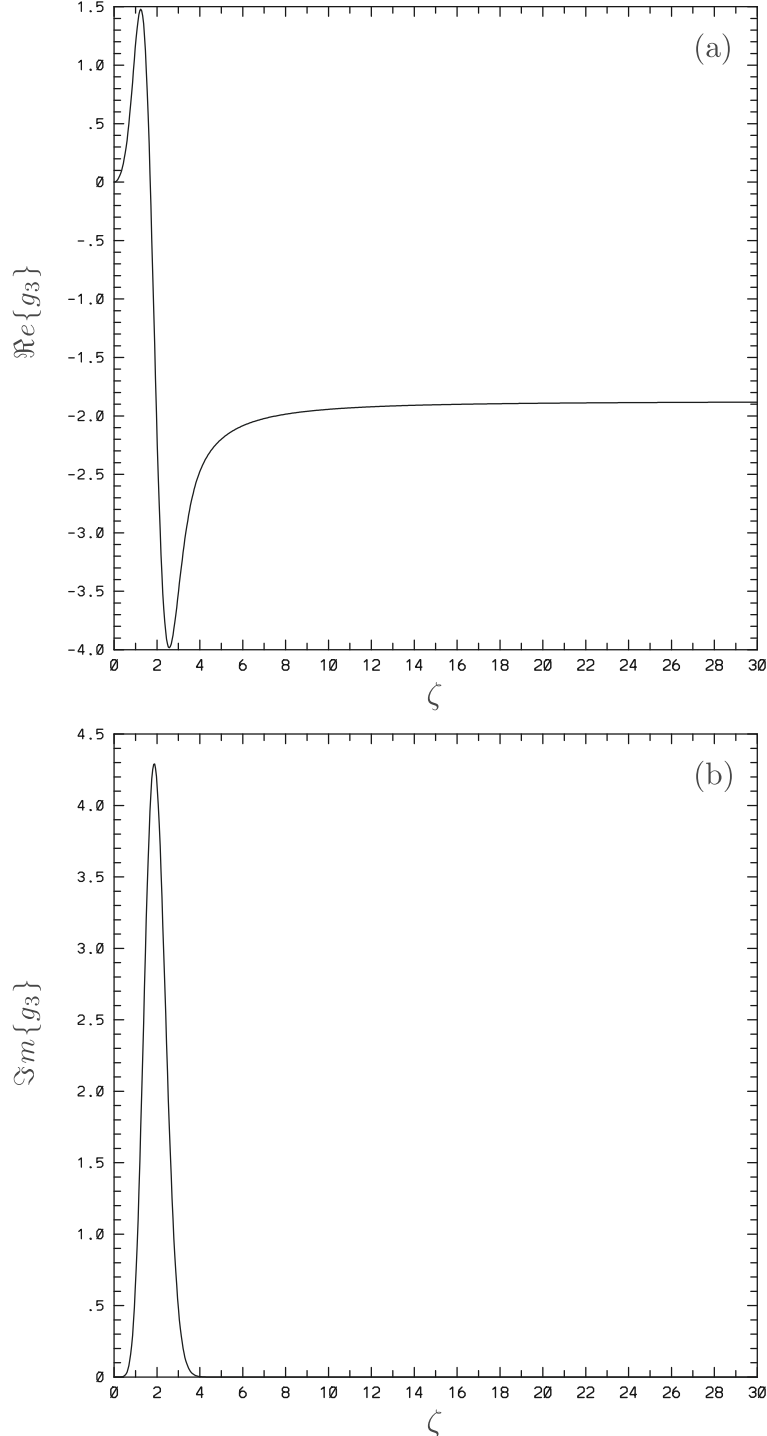

Fig. 1. The real (a) and imaginary (b) parts of the function $g_3(\zeta)$ as defined in Eq. (12) for real argument ζ.

We first describe the computation of the kinetic matrices. The kinetic effects reside in the following matrices: $\mathcal{A}_k, \mathcal{A}_k - i(n/\chi')\mathcal{B}_k, \mathcal{A}_k + i(n/\chi')\mathcal{B}_k^L, \mathcal{C}_k, \mathcal{C}_k^L, [\mathcal{A}_k + i(n/\chi')\mathcal{B}_k^L] + (n^2/\chi'^2)[\mathcal{D}_k - i(n/\chi')\mathcal{B}_k], \mathcal{E}_k - i(n/\chi')\mathcal{C}_k, \mathcal{E}_k^L + i(n/\chi')\mathcal{C}_k^L$, and $\mathcal{H}_k$. To determine these matrices, one needs to compute the ion pressure moment matrices: $\mathcal{P}_s, \mathcal{P}_{s1}, \mathcal{P}_0$, and the density moment matrices: $\mathcal{E}_s, \mathcal{E}_{s1}, \mathcal{E}_0$. In the previous section, we have shown that the energy integration can be dissociated and expressed
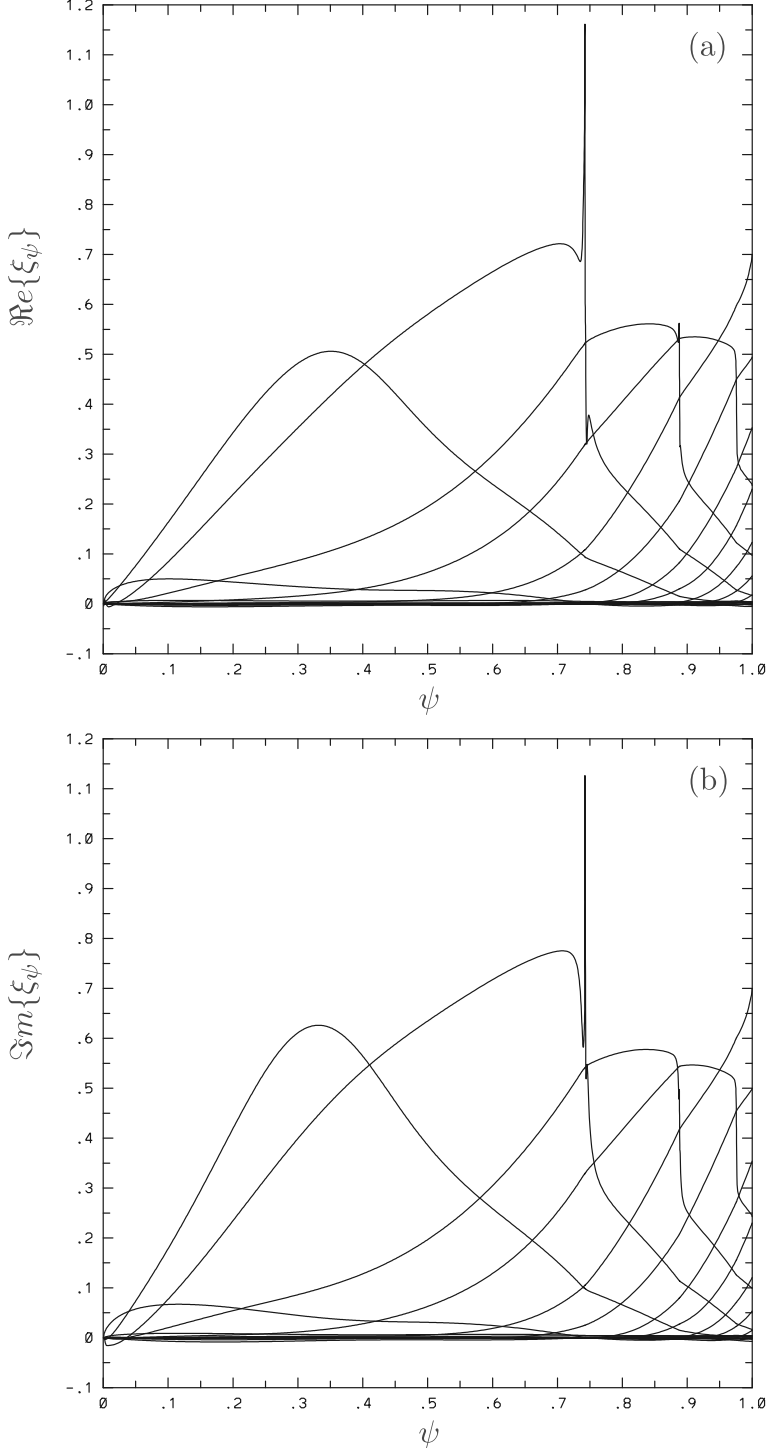
Fig. 2. The real (a) and imaginary (b) parts of the unstable RWM eigen mode as computed by the AEGIS-K code for ITER advanced scenario. The Hamada coordinates are employed for poloidal coordinate in this plot.

as the generalized Z-function $g_k(\zeta)$ ($k = 1, 2, 3$) in these kinetic moment matrices. Note that the function g_k is related to the plasma dispersion function and therefore can be bench marked. We compute g_k by using our Z-function code. Fig. 1(a) and (b) give, respectively the real and imaginary parts of $g_3(\zeta)$. As a benchmark, our double precision Z-function code is found to reproduce the 8 digit results in the Z-function table in Ref. [21]. Note that the wave-particle resonance effect is contained in g_k, our procedure can secure the accuracy in computing the wave-particle resonance effect. In our code, the values of the functions $g_k(\zeta)(k = 1, 2, 3)$ are tabulated and splined. This reduces the dimension of the integrations in computing the kinetic moment matrices.

Next, let us discuss the solution of the Euler–Lagrange Eq. (18). Due to our newly developed gyrokinetic formalism in Ref. [19] employed, the structure of the Euler–Lagrange Eq. (18) appears fluid-kinetic-hybrid-like, although our underlying formalism is fully kinetic. Therefore, we can extend the numerical scheme developed for MHD AEGIS code [7] to obtain the general solution for Eq. (18). We suppose the kinetic matrices are known in describing the solution. In Eq. (18) the Fourier decomposition has been performed in the poloidal direction. In the radial direction we solve for the general solution by using the decomposition based on the independent solutions in Eq. (19) and use the adaptive shooting scheme for independent solutions. The key difficulty to obtain the independent solutions lies in that each independent solution contains both the so-called large and small solutions at the mode resonance surfaces. If shooting directly from the magnetic axis to the plasma edge, the overall independent solutions are numerically polluted. To suppress the numerical pollution and get a better matrix condition, we employ a multiple region matching technique to get the overall independent solutions, as in the MHD AEGIS code. Indeed, we find that our numerical scheme combining the adaptive shooting and multiple region matching works also well for the current non-Hermitian problem.

Note that the kinetic eigen-value problem is complex and non-Hermitian. In generalizing the ideal MHD shooting procedure for real independent solutions in AEGIS code [19] to the current one for complex independent solutions, we make the real and imaginary parts to be balanced. This is achieved by setting the boundary conditions at the magnetic axis to be the same for real and imaginary parts, i.e., $\xi_{\psi,m} \propto r^m + ir^m$. This gives an opportunity to check the expansion from the original real formalism in MHD AEGIS code to the current complex problem in AEGIS-K code. Indeed, in the ideal MHD limit our AEGIS-K code yields the identical real and imaginary parts of the eigen functions which are both the same as that computed by AEGIS. We have also checked the fluid part of the AEGIS-K code with the case of pure continuum damping in the incompressible limit in Ref. [12]. An agreement is also found. This is because AEGIS-K code uses the same numerical formalism as that in Ref. [12]. From Appendix B one can see that, if the kinetic matrices ($\mathcal{A}_k, \mathcal{B}_k$, etc) are set to zero, AEGIS-K code becomes identical to the code used in Ref. [12].

AEGIS-K code can be used to study kinetic effects on various modes, for example resistive wall modes, peeling-ballooning modes, etc. Its application to resistive wall modes in ITER advanced scenario has been described in details in Ref. [14]. Here, we focus ourselves on discussing the numerical aspect of the application of AEGIS-K code. As Ref. [14], we consider an ITER advanced tokamak configuration and the $n = 1$ resistive wall modes. The numerical equilibrium is generated by the TOQ
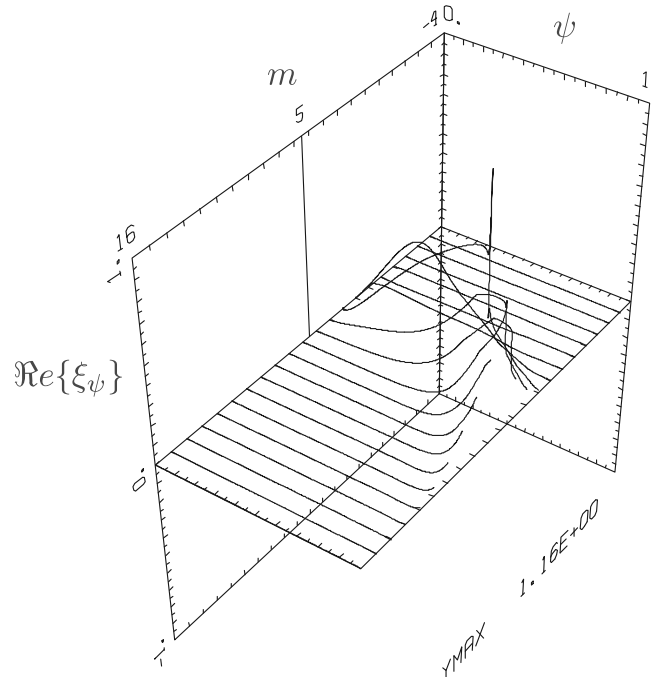

Fig. 3. Three dimensional re-plot of Fig. 2a, with the poloidal Fourier components displayed separately.

code. A typical equilibrium parameters are as follows: the normalized beta $\beta_N = 3.4, q_0 = 2.76, q_a = 5.39, q_{min} = 2.17, q_{95} = 4.22$, elongation $\kappa_a = 1.74$, and triangularity $\delta_a = 0.48$. Here, q_0, q_a, q_{min}, and q_{95} are respectively the safety factor values at the magnetic axis, the plasma edge, the q minimum, and the 95% radial flux surface. We consider the conformal wall with the wall position $b = 1.5$ normalized by the plasma minor radius. As discussed in the last section, for the RWM problem, the reduced eigen-value problem in Eq. (33) can be used to study the stability. The the real and imaginary parts of the eigen function for the normalized rotation frequency $\Omega = 0.005$ (normalized by the Alfvén frequency at magnetic axis
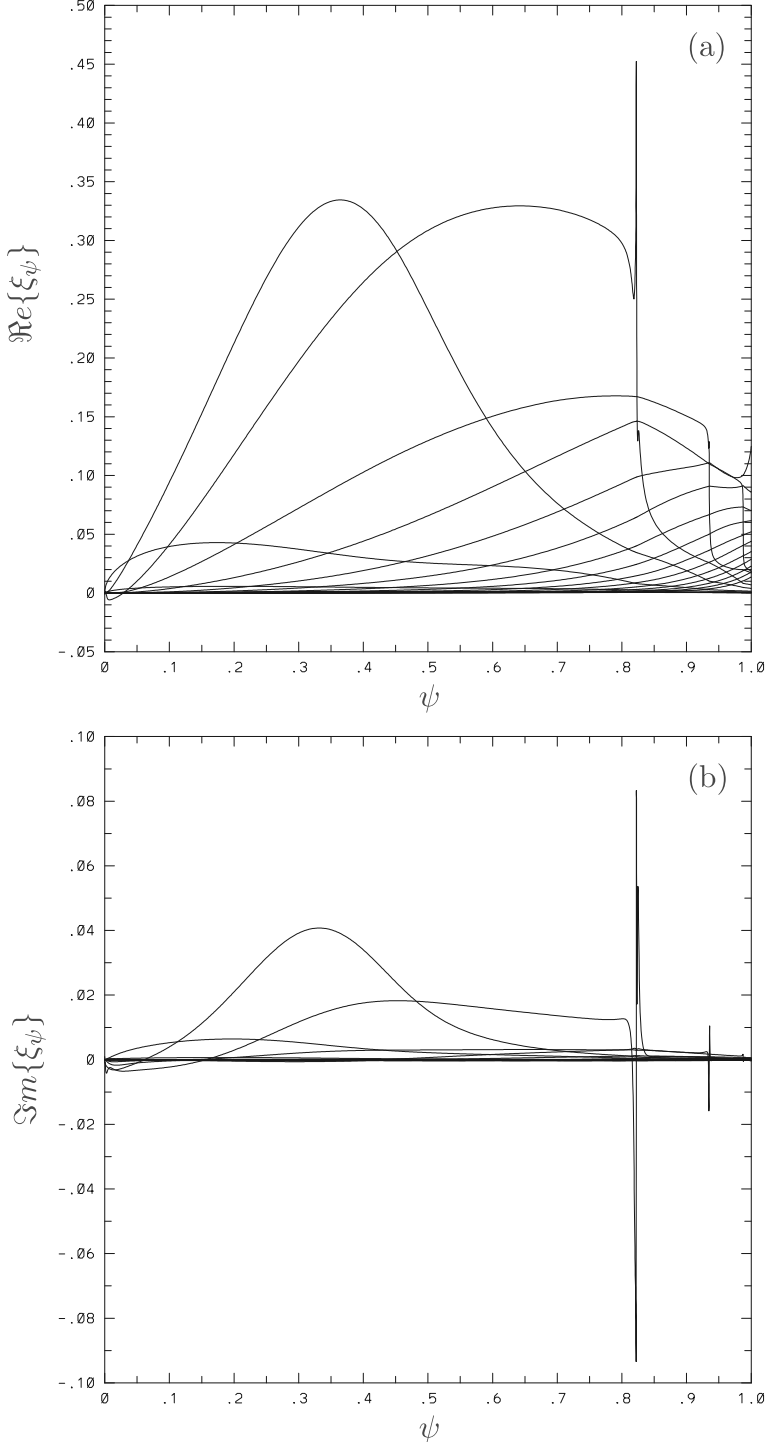
Fig. 4. The re-plots of Fig. 2 in the PEST coordinates and with redefined real $[(\xi_r + \xi_i)/2]$ and imaginary $[(\xi_i - \xi_r)/2]$ parts.

V_A/Rq) are plotted in Fig. 2(a) and (b), in which the Hamada coordinates are employed. The eigen-value for this case is $\tau_w\gamma_N = 10.08$. Fig. 3 is the three dimensional plot of Fig. 2(a), with the poloidal Fourier components displayed separately. As shown in Fig. 3 a good poloidal convergency can be achieved generally by about 20 poloidal Fourier components for $n = 1$ modes. It is found that for even smaller rotation frequency, the eigen function becomes closer to that of purely continuum damping case [12]. This is because the strength of the wave-particle resonance effect depends on the number of the resonance particles. The smaller the rotation frequency, the less the number of the resonance particles.
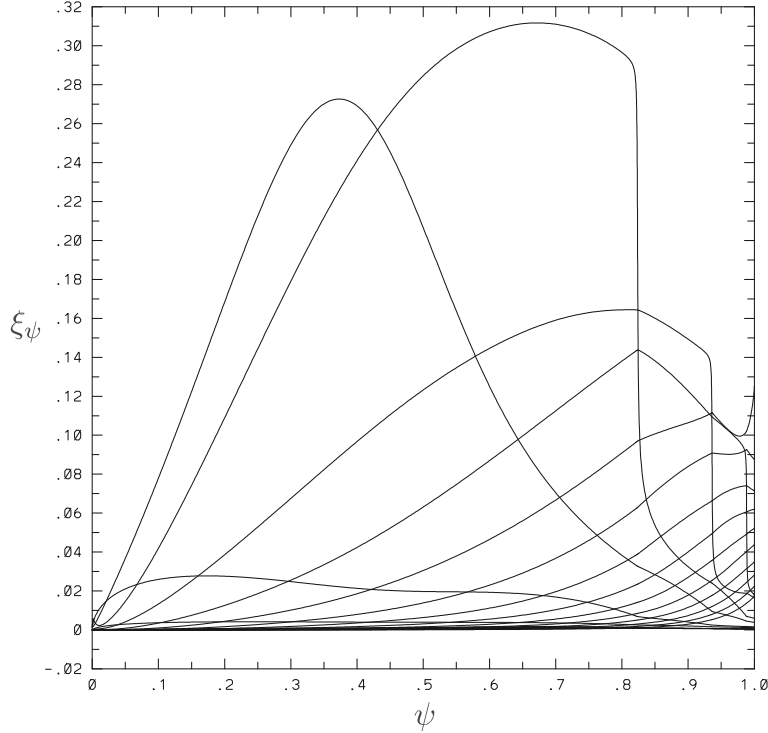
Fig. 5. The ideal MHD eigen mode for same equilibrium and coordinate system as Fig. 4a as computed by AEGIS.
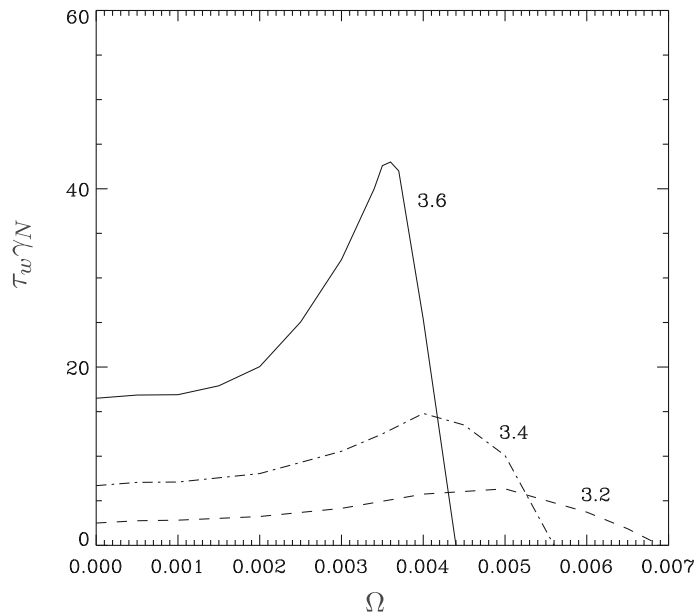

Fig. 6. RWM growth rate $\tau_w\gamma_N$ versus normalized rotation frequency Ω with beta normal β_N as parameters.

To compare with the ideal MHD case, we transform Fig. 2(a) and (b) from the Hamada coordinates to the PEST coordinates and multiply the eigen function with a normalization constant $(1 - i)/2$ (which corresponds to the boundary conditions at the magnetic axis: $\xi_{\psi,m} \propto r^m + i0$). The transformed results are plotted in Fig. 4(a) and (b). When kinetic and Alfvén resonances are removed, the solution becomes completely real. Therefore, the curves Fig. 4(b) are just reduced to zero and those in Fig. 4(a) becomes exactly the MHD eigen function in Fig. 5 as computed by AEGIS or GATO codes. With the kinetic resonance taken into account, the modulation due to g_k at each side of the mode rational surfaces appears in the eigen functions. We have also checked our formalism and code for recovering the MHD apparent mass effect in the large aspect ratio limit. In this limit, the perpendicular inertia is given by the term $\hat{\gamma}_N^2 \mathcal{A}_k$ in $\mathcal{F}$, which equals to $\hat{\gamma}_N^2(1/Rq_0^2)$ in the large aspect ratio limit. The apparent mass term is present in the term $[\mathcal{A}_k + i(n/\chi')\mathcal{B}_k^L] + (n^2/\chi'^2)[\mathcal{D}_k - i(n/\chi')\mathcal{B}_k]$ also in $\mathcal{F}$. In the large aspect ratio limit, $[\mathcal{D}_k - i(n/\chi')\mathcal{B}_k]$ becomes negligibly small and the reminding term is as follows $\mathcal{A}_c + i(n/\chi')\mathcal{B}_c^L = (4/3)\hat{\gamma}_N^2(1/Rq_0^2)2q^2$. This gives exactly the MHD apparent mass term, except the factor 4/3. As proved in Ref. [7], this factor results from the collisionless description in the parallel direction in the AEGIS-K code, as compared with the MHD adiabatic assumption.

As shown in Ref. [14], AEGIS-K computation predicts that the resistive wall modes in ITER advanced scenario can be stabilized by a modestly low rotation. Fig. 6 shows the further details about the rotation stabilization of resistive wall modes in ITER advanced scenario as given in Ref. [14]. In Fig. 6, the normalized RWM growth rates are plotted versus the normalized rotation frequency. Three different values (3.2, 3.4, and 3.6) of beta normal are given in Fig. 6. The beta normal values for no wall and for perfectly conducting wall are respectively 2.95 and 3.84. From Fig. 6, one can see that the RWM growth rate initially increases with the rotation frequency when rotation frequency is small, but later decreases when rotation frequency is sufficiently large. Fig. 6 also shows that RWMs in ITER advanced scenario can be fully stabilized by modestly low rotation. The higher the beta normal, the lower the rotation frequency required for full stabilization. Here, we note that AEGIS-K code in its current version has not taken into account the finite Larmor radius effects, especially those related to the resonances with ion precessional drift [17]. Therefore, the low rotation results in Fig. 6 requires to include more subtle physics. But, the results with modestly low rotation (larger than ion diamagnetic frequency), predicted for full stabilization of resistive wall modes, are unaffected [14].

Currently, we have run AEGIS-K code at IBM p575 POWER 5 computer system BASSI at National Energy Research Scientific Computing Center, which is composed of 1.9 GHz POWER 5 processors. For determining a RWM eigen mode for ITER type of configuration with up-down symmetry, it takes about 20 h with single processor. Most of computing time spent in AEGIS-K is used to compute kinetic matrices ($\mathcal{A}_k$, etc.) at about 800 radial grid points packed at the rational surfaces. We believe further optimization of the code is possible.

5. Conclusions and discussion

In this paper we describe the AEGIS-K code and its numerical scheme for computing the tokamak stability in the kinetic formalism. Our work improves the global numerical computation of the kinetic effects on the MHD modes both from the underlying theoretical formalism and the numerical scheme.

In the theoretical formulation we are able to avoid the hybrid formulation and the perturbative method, used widely in this field. This attributes to that the AEGIS-K formalism is based on our newly developed gyrokinetic theory in Ref. [19]. One of the important features of our newly developed gyrokinetics lies in the recovery of the full MHD in the proper limit. By exploiting this feature, our AEGIS-K code is constructed as a fully kinetic code and nevertheless with a hybrid appearance. This makes our kinetic investigation of the global MHD modes to have kept the MHD root. This is not trivial. Very easily a fully kinetic or nonhybdrid computation of the MHD modes ends up with losing MHD trace, so that it is hardly to tell the correctness of the numerical results. The vigor of the MHD trace lies in that it reflects the particle localization by the strong magnetic field. In the AEGIS-K code we have taken into account the following non-MHD effects: (1) the coupling of kinetic resonances with the continuum damping, (2) the parallel electric effects, and (3) the trapped particle effects. Our procedure is based on the self-consistent investigation of the eigen value problem, instead of the perturbative method.

In the numerical scheme we are able to compute the kinetic effects on the MHD modes with an adaptive numerical scheme. This is important since there is coupling between the Alfvén continuum damping and kinetic resonances. High resolution computation is required to resolve this coupling. We extend the adaptive shooting scheme in the AEGIS code for real MHD stability problem to treat the current complex and non-Hermitian kinetic stability problem in the AEGIS-K code. We develop a numerical scheme based on the independent solution method to solve the integro-differential gyrokinetic equation, in which the parallel electric field effect included. In computing the kinetic resonance effect, we develop a coordinate transform so that the Z-function can used directly to compute the pressure moment. This assures the computation accuracy of the wave-particle resonance effects and also speeds up the computing time. In the treatment of the trapped particle effect we introduce the periodic boundary condition around the banana orbit. This unifies the treatment of the circulating and trapped particles. In general the Nyquist diagram is needed to determine the stability. However, in the RWM case a simplified eigen-value problem can be developed. As a showcase of the AEGIS-K code application, we present our calculation for the kinetic effects on RWMs in the ITER advanced tokamak scenario.

Our AEGIS-K code is an useful tool for studying the tokamak global stabilities with kinetic effects included, for example RWMs [14]. The applicable frequency domain of the AEGIS-K code lies in between the ion diamagnetic drift and the electron transit frequencies. As AEGIS-K code keeps the main feature of the AEGIS, it can be used to study both low and medium high n modes. In our current effort the FLR effects have not been included, especially the precessional drift resonance effect [13]. We propose it as a future research.

Acknowledgements

Appendix A. Definitions of the matrices in Eqs. (15) and (16)

The equilibrium matrices in Euler–Lagrange equations, Eqs. (15) and (16), are consist of three parts: the MHD part (denoted by subscript "f", which is DCON-like [6]), the inertia part (denoted by subscript "i"), and the kinetic part (denoted by subscript "k"), for example

$$\mathcal{A} = \mathcal{A}_f + \hat{\gamma}_N^2 \mathcal{A}_i + \mathcal{A}_k.$$

Here, the MHD matrices are given as follows

$$\mathcal{A}_f = n(n\mathcal{G}_{22} + \mathcal{G}_{23}\mathcal{M}) + \mathcal{M}(n\mathcal{G}_{23} + \mathcal{G}_{33}\mathcal{M}),$$
$$\mathcal{B}_f = -i\chi'[n(\mathcal{G}_{22} + q\mathcal{G}_{23}) + \mathcal{M}(\mathcal{G}_{23} + q\mathcal{G}_{33})],$$
$$\mathcal{C}_f = -i[\chi''(n\mathcal{G}_{22} + \mathcal{M}\mathcal{G}_{23}) + (q\chi')'(n\mathcal{G}_{23} + \mathcal{M}\mathcal{G}_{33})] - \chi'(n\mathcal{G}_{12} + \mathcal{M}\mathcal{G}_{31})\mathcal{Q} + i(g'\mathcal{Q} - \mu_0 nP'\mathcal{J}/\chi'),$$
$$\mathcal{D}_f = \chi'^2[(\mathcal{G}_{22} + q\mathcal{G}_{23}) + q(\mathcal{G}_{23} + q\mathcal{G}_{33})],$$
$$\mathcal{E}_f = \chi'[\chi''(\mathcal{G}_{22} + q\mathcal{G}_{23}) + (q\chi')'(\mathcal{G}_{23} + q\mathcal{G}_{33})] - i\chi'^2(\mathcal{G}_{12} + q\mathcal{G}_{31})\mathcal{Q} + \mu_0 P'\mathcal{J},$$
$$\mathcal{H}_f = \chi''[\chi''\mathcal{G}_{22} + (q\chi')'\mathcal{G}_{23}] + (q\chi')'[\chi''\mathcal{G}_{23} + (q\chi')'\mathcal{G}_{33}] + i\chi'[\chi''(\mathcal{M}\mathcal{G}_{12} - \mathcal{G}_{12}\mathcal{M}) + (q\chi')'(\mathcal{M}\mathcal{G}_{31} - \mathcal{G}_{31}\mathcal{M})]$$
$$+ \chi'^2\mathcal{Q}\mathcal{G}_{11}\mathcal{Q} + \mu_0 P'\chi''\mathcal{J}/\chi' + \mu_0 P'\mathcal{J}' - g'q'\chi'\mathcal{I},$$

where $\mathcal{M}_{mm'} = m\mathcal{I}_{mm'}$ and $\mathcal{Q}_{mm'} = (m - nq)\mathcal{I}_{mm'}$. The perpendicular inertia matrices are as follows

$$\mathcal{A}_i = \frac{B_0^2}{X_0^2 q_0^2} \left\langle \mathcal{J}\frac{\rho_N}{B^2}|\nabla\psi|^2 \right\rangle,$$
$$\mathcal{C}_i = \frac{B_0^2}{X_0^2 q_0^2} \left\langle \chi'\mathcal{J}\frac{\rho_N}{B^2}(\nabla\psi \cdot \nabla\zeta - q\nabla\psi \cdot \nabla\theta) \right\rangle,$$
$$\mathcal{H}_i = \frac{B_0^2}{X_0^2 q_0^2} \left\langle \chi'^2\mathcal{J}\frac{\rho_N}{B^2}(|\nabla\zeta|^2 + q^2|\nabla\theta|^2 - 2\nabla\theta \cdot \nabla\zeta) \right\rangle,$$

where ρ_N is the dimensionless mass density normalized by the mass density at the magnetic axis. The kinetic matrices are as follows

$$\mathcal{A}_k = i\mu_0 n_0 T_i \frac{1}{q}\left[\frac{1}{\chi'}\langle\mathcal{J}\rangle\mathcal{M} - \chi'\left\langle\frac{1}{B^2}(G_{22} + qG_{23})\right\rangle\mathcal{Q}\right]\langle\mathcal{P}_s + \mathcal{P}_\varphi\mathcal{E}_\varphi^{-1}\mathcal{E}_s\rangle,$$
$$\mathcal{B}_k = i\mu_0 n_0 T_i \frac{1}{q}\left[\frac{1}{\chi'}\langle\mathcal{J}\rangle\mathcal{M} - \chi'\left\langle\frac{1}{B^2}(G_{22} + qG_{23})\right\rangle\mathcal{Q}\right]\langle\mathcal{P}_1 + \mathcal{P}_\varphi\mathcal{E}_\varphi^{-1}\mathcal{E}_1\rangle,$$
$$\mathcal{C}_k = i\mu_0 n_0 T_i \frac{1}{q}\left[\frac{1}{\chi'}\langle\mathcal{J}\rangle\mathcal{M} - \chi'\left\langle\frac{1}{B^2}(G_{22} + qG_{23})\right\rangle\mathcal{Q}\right]\langle\mathcal{P}_0 + \mathcal{P}_\varphi\mathcal{E}_\varphi^{-1}\mathcal{E}_0\rangle,$$
$$\mathcal{B}_k^L = -\mu_0 n_0 T_i\langle\mathcal{J}\rangle\langle\mathcal{P}_s + \mathcal{P}_\varphi\mathcal{E}_\varphi^{-1}\mathcal{E}_s\rangle,$$
$$\mathcal{D}_k = -\mu_0 n_0 T_i\langle\mathcal{J}\rangle\langle\mathcal{P}_1 + \mathcal{P}_\varphi\mathcal{E}_\varphi^{-1}\mathcal{E}_1\rangle,$$
$$\mathcal{E}_k = -\mu_0 n_0 T_i\langle\mathcal{J}\rangle\langle\mathcal{P}_0 + \mathcal{P}_\varphi\mathcal{E}_\varphi^{-1}\mathcal{E}_0\rangle,$$
$$\mathcal{C}_k^L = \mu_0 n_0 T_i\left[i\chi'^2\left\langle\frac{1}{B^2}(G_{12} + qG_{31})\right\rangle\mathcal{Q} + \langle\mathcal{J}'\rangle\right]\langle\mathcal{P}_s + \mathcal{P}_\varphi\mathcal{E}_\varphi^{-1}\mathcal{E}_s\rangle,$$
$$\mathcal{E}_k^L = \mu_0 n_0 T_i\left[i\chi'^2\left\langle\frac{1}{B^2}(G_{12} + qG_{31})\right\rangle\mathcal{Q} + \langle\mathcal{J}'\rangle\right]\langle\mathcal{P}_1 + \mathcal{P}_\varphi\mathcal{E}_\varphi^{-1}\mathcal{E}_1\rangle,$$
$$\mathcal{H}_k = \mu_0 n_0 T_i\left[i\chi'^2\left\langle\frac{1}{B^2}(G_{12} + qG_{31})\right\rangle\mathcal{Q} + \langle\mathcal{J}'\rangle\right]\langle\mathcal{P}_0 + \mathcal{P}_\varphi\mathcal{E}_\varphi^{-1}\mathcal{E}_0\rangle.$$

Here, we note that the superscript L represents just the Hermitian conjugate for MHD and inertia parts of matrices.

Appendix B. Simplification of matrices in Eq. (17)

The matrices in Eq. (17) can be further simplified as follows

$$\mathcal{F} = \frac{\chi'^2}{n^2}\left\{ \mathcal{Q}\mathcal{G}_{33}\mathcal{Q} + \hat{\gamma}_N^2\mathcal{A}_i + \left(\mathcal{A}_k + i\frac{n}{\chi'}\mathcal{B}_k^L\right) + \frac{n^2}{\chi'^2}\left(\mathcal{D}_k - i\frac{\chi'}{n}\mathcal{B}_k\right)\right.$$

$$- \left[\hat{\gamma}_N^2\mathcal{A}_i + \left(\mathcal{A}_k + i\frac{n}{\chi'}\mathcal{B}_k^L\right) + \mathcal{Q}(n\mathcal{G}_{23} + \mathcal{G}_{33}\mathcal{M})\right]$$

$$\left.\times \mathcal{A}^{-1}\left[\hat{\gamma}_N^2\mathcal{A}_i + \left(\mathcal{A}_k - i\frac{n}{\chi'}\mathcal{B}_k\right) + (n\mathcal{G}_{23} + \mathcal{M}\mathcal{G}_{33})\mathcal{Q}\right]\right\},$$

$$\mathcal{K} = \frac{\chi'}{n}\left\{ i\left[\hat{\gamma}_N^2\mathcal{A}_i + \left(\mathcal{A}_k + i\frac{n}{\chi'}\mathcal{B}_k^L\right) + \mathcal{Q}(n\mathcal{G}_{23} + \mathcal{G}_{33}\mathcal{M})\right]\mathcal{A}^{-1}\mathcal{C}\right.$$

$$\left.- \mathcal{Q}[\chi''\mathcal{G}_{23} + (q\chi')'\mathcal{G}_{33} - i\chi'\mathcal{G}_{31}\mathcal{Q} - g'\mathcal{I}] - i\hat{\gamma}_N^2\mathcal{C}_i\right\} + \left(\mathcal{E}_k - i\chi'\frac{1}{n}\mathcal{C}_k\right),$$

$$\mathcal{K}^L = \frac{\chi'}{n}\left\{ -i\mathcal{C}^L\mathcal{A}^{-1}\left[\hat{\gamma}_N^2\mathcal{A}_i + \left(\mathcal{A}_k - i\frac{n}{\chi'}\mathcal{B}_k\right) + (n\mathcal{G}_{23} + \mathcal{M}\mathcal{G}_{33})\mathcal{Q}\right]\right.$$

$$\left.- [\chi''\mathcal{G}_{23} + (q\chi')'\mathcal{G}_{33} + i\chi'\mathcal{Q}\mathcal{G}_{31} - g'\mathcal{I}]\mathcal{Q} + i\hat{\gamma}_N^2\mathcal{C}_i\right\} + \left(\mathcal{E}_k^L + i\chi'\frac{1}{n}\mathcal{C}_k^L\right).$$

Here, the MHD part simplification is DCON-like [6]. In these matrices, the kinetic parts can be further combined as follows

$$\mathcal{A}_k - i\frac{n}{\chi'}\mathcal{B}_k = i\mu_0 n_0 T_i \frac{1}{q}\left[\frac{1}{\chi'}\langle\mathcal{J}\rangle\mathcal{M} - \chi'\left\langle\frac{1}{B^2}(G_{22} + qG_{23})\right\rangle\mathcal{Q}\right]\langle\mathcal{P}_{s1} + \mathcal{P}_\varphi\mathcal{E}_\varphi^{-1}\mathcal{E}_{s1}\rangle,$$

$$\mathcal{A}_k + i\frac{n}{\chi'}\mathcal{B}_k^L = i\mu_0 n_0 T_i \frac{1}{q}\left[\frac{1}{\chi'}\langle\mathcal{J}\rangle\mathcal{Q} - \chi'\left\langle\frac{1}{B^2}(G_{22} + qG_{23})\right\rangle\mathcal{Q}\right]\langle\mathcal{P}_s + \mathcal{P}_\varphi\mathcal{E}_\varphi^{-1}\mathcal{E}_s\rangle,$$

$$\left(\mathcal{A}_k + i\frac{n}{\chi'}\mathcal{B}_k^L\right) + \frac{n^2}{\chi'^2}\left(\mathcal{D}_k - i\frac{\chi'}{n}\mathcal{B}_k\right) = i\mu_0 n_0 T_i \frac{1}{q}\left[\frac{1}{\chi'}\langle\mathcal{J}\rangle\mathcal{Q} - \chi'\left\langle\frac{1}{B^2}(G_{22} + qG_{23})\right\rangle\mathcal{Q}\right]\langle\mathcal{P}_{s1} + \mathcal{P}_\varphi\mathcal{E}_\varphi^{-1}\mathcal{E}_{s1}\rangle,$$

$$\mathcal{E}_k - i\chi'\frac{1}{n}\mathcal{C}_k = \mu_0 n_0 T_i \frac{1}{nq}\left[\langle\mathcal{J}\rangle\mathcal{Q} - \chi'^2\left\langle\frac{1}{B^2}(G_{22} + qG_{23})\right\rangle\mathcal{Q}\right]\langle\mathcal{P}_0 + \mathcal{P}_\varphi\mathcal{E}_\varphi^{-1}\mathcal{E}_0\rangle,$$

$$\mathcal{E}_k^L + i\chi'\frac{1}{n}\mathcal{C}_k^L = i\mu_0 n_0 T_i \frac{\chi'}{n}\left[i\chi'^2\left\langle\frac{1}{B^2}(G_{12} + qG_{31})\right\rangle\mathcal{Q} + \langle\mathcal{J}'\rangle\right]\langle\mathcal{P}_{s1} + \mathcal{P}_\varphi\mathcal{E}_\varphi^{-1}\mathcal{E}_{s1}\rangle,$$

where $\mathcal{P}_{s1} = \mathcal{P}_s - i(n/\chi')\langle\mathcal{P}_1\rangle$ and $\mathcal{E}_{s1} = \mathcal{E}_s - i(n/\chi')\langle\mathcal{E}_1\rangle$.

References

[1] R.C. Grimm, J.M. Greene, J.L. Johnson, Methods of Computational Physics, vol. 9, Academic Press, New York, London, 1976. pp. 253–280.
[2] M.S. Chance, J.M. Greene, R.C. Grimm, J.L. Johnson, W. Kerner, D. Berger, L.C. Bernard, R. Gruber, F.J. Troyon, Comparative numerical studies of ideal magnetohydrodynamic instabilities, J. Comput. Phys. 28 (1978) 1–13.
[3] R. Gruber, F. Troyon, D. Berger, L.C. Bernard, S. Roussert, R. Schreiber, W. Kerner, W. Schneider, K.V. Roberts, ERATO stability code, Comput. Phys. Commun. 22 (1981) 323–377.
[4] R. Gruber, F. Troyon, S. Roussert, W. Kerner, L.C. Bernard, Transform of ERATO into a δW code, Comput. Phys. Commun. 22 (1981) 383–387.
[5] L.C. Bernard, F.J. Helton, R.W. Moore, GATO: an MHD stability code for axisymmetric plasmas with internal separatrices, Comput. Phys. Commun. 24 (1981) 377–380.
[6] A.H. Glasser, The direct criterion of Newcomb for the Stability of an Axisymmetric Toroidal Plasma, Los Alamos Report LA-UR-95-528, 1997.
[7] L.-J. Zheng, M. Kotschenreuther, AEGIS: an adaptive ideal-magnetohydrodynamics shooting code for axisymmetric plasma stability, J. Comput. Phys. 221 (2006) 748–766.
[8] S. Tokuda, T. Watanabe, A new eigen-value problem associated with the two-dimensional Newcomb equation without continuous spectra, Phys. Plasmas 6 (1999) 3012–3026.
[9] A.B. Mikhalovskii, G.T.A. Huysmans, S.E. Sharapov, W. Kerner, Optimization of computational MHD normal mode analysis for tokamaks, Plasma Phys. Rep. 23 (1997) 844–857.
[10] A. Bondeson, D.J. Ward, Stabilization of external modes in tokamaks by resistive walls and plasma rotation, Phys. Rev. Lett. 72 (1994) 2709–2712.
[11] R. Betti, J.P. Freidberg, Stability analysis of resistive wall kink modes in rotating plasmas, Phys. Rev. Lett. 74 (1995) 2949–2952.
[12] L.J. Zheng, M. Kotschenreuther, M. Chu, Rotational stabilization of resistive wall modes by the shear Alfvén resonance, Phys. Rev. Lett. 95 (2005) 255003.
[13] B. Hu, R. Betti, Resistive wall mode in collisionless quasistationary plasmas, Phys. Rev. Lett. 93 (2004) 105002.
[14] L.J. Zheng, M.T. Kotschenreuther, J.W. Van Dam, Kinetic analysis of the resistive wall modes in ITER advanced tokamak scenario, Nucl. Fusion 49 (2009) 075021.
[15] C.Z. Cheng, Kinetic extensions of magnetohydrodynamics for axisymmetric toroidal plasmas, Phys. Rep. 211 (1992) 1–51.
[16] S.D. Pinches, L.C. Appel, J. Candy, S.E. Sharapov, H.L. Berk, D. Borba, B.N. Breizman, T.C. Hender, K.I. Hopcraft, G.T.A. Huysmans, W. Kerner, The HAGIS self-consistent nonlinear wave–particle interaction model, Comput. Phys. Commun. 111 (1998) 133–149.
[17] B. Hu, R. Betti, J. Manickam, Application of the low-frequency energy principle to wall modes, Phys. Plasmas 12 (2005) 057301.

[18] Yueqiang Liu, M.S. Chu, I.T. Chapman, T.C. Hender, Toroidal self-consistent modeling of drift kinetic effects on the resistive wall mode, Phys. Plasmas 15 (2008) 112503.
[19] L.J. Zheng, M.T. Kotschenreuther, J.W. Van Dam, Revisiting linear gyrokinetics to recover ideal magnetohydrodynamics and missing finite Larmor radius effects, Phys. Plasmas 14 (2007) 072505.
[20] L. Degtyarev, A. Martinov, S. Medvedev, F. Troyon, L. Villard, R. Gruber, Iterative solution of global electromagnetic wavefields with finite elements, Comput. Phys. Commun. 103 (1997) 10–27.
[21] B.D. Fried, The Plasma Dispersion Function, Physical Research Laboratory, Space Technology Laboratories, 1960.
[22] S. Hamada, Hydromagnetic equilibria and their proper coordinates, Nucl. Fusion 2 (1962) 23–37.
[23] M.S. Chance, Vacuum calculations in azimuthally symmetric geometry, Phys. Plasmas 4 (1997) 2161–2180.